Folding of graphene slit like pore walls—a simple method of improving CO2 separation from mixtures with CH4 or N2

Article

Accepted Version

Folding of graphene slit like pore walls—a simple method of improving CO_2 separation from mixtures with CH_4 or N_2

Sylwester Furmaniak[1*], Artur P. Terzyk[1], Piotr A. Gauden[1], Piotr Kowalczyk[2] and Peter J.F. Harris[3]

[1] Department of Chemistry, Physicochemistry of Carbon Materials Research Group, N. Copernicus University, Gagarin St. 7, 87-100 Toruń, Poland

[2] Nanochemistry Research Institute, Department of Chemistry, Curtin University of Technology, P.O. Box U1987, Perth, 6845 Western Australia, Australia

[3] Electron microscopy laboratory, University of Reading, Whiteknights, Reading RG6 6AF, UK

* corresponding author:
Sylwester Furmaniak
e-mail: sf@chem.umk.pl
tel. (+48) (56) 611-44-27
fax: (+48) (56) 654-24-77
url: http://www.chem.umk.pl/~aterzyk

Abstract

We report for the first time a detailed procedure for creating a simulation model of energetically stable, folded graphene-like pores and simulation results of CO_2/CH_4 and CO_2/N_2 separation using these structures. We show that folding of graphene structures is a very promising method to improve the separation of CO_2 from mixtures with CH_4 and N_2. The separation properties of the analyzed materials are compared with carbon nanotubes having similar diameters or *S/V* ratio. The presented results have potential importance in the field of CO_2 capture and sequestration.

Keywords

Graphene folded pores, GCMC simulation, carbon dioxide separation, adsorption

1. Introduction

It is well known that CO_2 capture from different gas mixtures is an environmentally important problem. It concerns among other things the removal of CO_2 from natural gas or biogas and the CO_2 capture and sequestration from flue gases. We have shown recently, that when choosing the most effective adsorbent for this purpose two parameters should be considered namely: surface to volume ratio, and the energy of adsorption [1]. Both factors should be as large as possible to obtain high CO_2 separation factors.

Among the carbonaceous structures available for this application, the so called folded graphene structures seem to have particular promise [2-5]. Very interesting results in this field have been published by Liu et al. [6] who described the existence of this type of structures in the heat treated graphite. Folded bilayer graphene exhibits AA - stacking of layers. Zhang et al. [7] demonstrated that this type of structures can be obtained during the process of graphene ultrasonication, and Ju et al. [8] studied theoretically thermal conductivity of folded graphene. Kim et. al. [9] presented experimental results that folded structures in graphene, termed grafold, exist, and their formations can be controlled by introducing anisotropic surface curvature during graphene synthesis or transfer processes. Moreover, those authors using pseudopotential-density-functional-theory calculations, shown that double folding modifies the electronic band structure of graphene. Lopez-Bezanilla et al. [10] compared experimental images of stable closed-edge structures in few-layer graphene samples obtained by high-resolution transmission electron microscopy (HRTEM) with first principles density functional theory calculations. Dutta et al. [11] stated using van-der-Waals-corrected density functional

theory calculations that the differential between the adsorption of CO_2 and CH_4 is much higher on folded graphene sheets and at concave curvatures; this could possibly be leveraged for CH_4/CO_2 flow separation and gas selective sensors.

The discovery of folded graphene shows that the synthesis of carbon membranes containing folded graphene slit-like pores is plausible and it is interesting to investigate adsorption properties of this type of structures. Thus following our previous findings [1,12,13] the purpose of the current study is to check, using the GCMC simulation method, the influence of slit-like pore walls folding on separation properties. The results are compared with those calculated for carbon nanotubes. Our results demonstrate that folded graphene structures can very efficiently separate CO_2 from mixtures with CH_4 or N_2.

2. Calculation details

2.1 Folded graphene sheets and simulation boxes

To perform simulation we propose a new procedure to generate folded graphene sheets. All the considered graphene sheets were generated from a flat sheet (presented on Fig. 1a) having a size of 10.2572×4.23 nm with periodic boundary conditions in *x* and *z* directions. This plane was folded in the *y* direction according to the equation:

$$y(x) = A \times \sin\left(\frac{2\pi n x}{L_{box,x}(A)}\right) \qquad (1)$$

where *A* is the amplitude (maximal deviation from the initial position), *n* is the integer number (we assumed $n = 2$) and $L_{box,x}(A)$ is the length of the box in *x* direction after folding for the given *A* value. The following amplitude values are considered: $A = 0.00$, 0.25, 0.50, 0.75, and 1.00 nm. In order to maintain the starting length of the sheet during the folding process (which is necessary to prevent the stretching C-C bond lengths) the length of folded plane should be the same as the initial one (i.e. the length of the box with flat surface for A = 0 (i.e. $L_{box,x}(A=0)$)). This condition causes the reduction in the length of the boxes for folded sheets ($L_{box,x}(A\neq 0)$). The length of the curve (defined by Eq. (1)) may be calculated *via* the integration. Hence, $L_{box,x}(A)$ should fulfil the equation:

$$L_{box,x}\left(A=0\right)=\int_{-\frac{1}{2}L_{box,x}(A)}^{\frac{1}{2}L_{box,x}(A)}\sqrt{1+\left(\frac{dy}{dx}\right)^2}\,dx=\int_{-\frac{1}{2}L_{box,x}(A)}^{\frac{1}{2}L_{box,x}(A)}\sqrt{1+\frac{4\pi^2n^2A^2}{\left(L_{box,x}\left(A\right)\right)^2}\times\cos^2\left(\frac{2\pi nx}{L_{box,x}\left(A\right)}\right)}dx \qquad (2)$$

This equation is new and, to our knowledge, has not been published before. For each considered A value the length of the box ($L_{box,x}(A)$) is find using a bisection procedure and numerical integration. Fig. 1b shows all the considered folded graphene sheets generated following Eq. (2) and calculated values of $L_{box,x}(A)$.

Despite the fact that applied procedure of sheets folding is similar to theoretical generating of nanotubes by graphene folding [15] (and, in consequence, it does not vitally affect the bonds lengths) we decide to relax the geometrically generated folded sheets. The relaxation is realised using simple Metropolis Monte Carlo simulation in canonical ensemble [16] employing one of the most sophisticated carbon force field, i.e., carbon EDIP potential proposed by Marks [17,18]. The computation scheme is similar to one previously described [19]. For each sheet 600 simulation cycles are performed. During each cycle $100\times N_C$ (where N_C is the number of C atoms) attempts of the change of the system state (*via* the random displacement of randomly chosen atom) are performed. The temperature is changed during the simulation (see Fig. S1a in Supplementary data). It is equal to 1000 K for the first 100 cycles. Next it is linearly reduced down to 100 K during 400 cycles and, finally, the last 100 cycles are performed for a constant temperature equal to 100 K.

Thermodynamically equilibrated sheets generated in this way (Fig. 1c) are used for the preparation of simulation boxes composed of slit-like pores. As in our previous study [20], we consider multiplied slits system in a cubicoid box with periodic boundary conditions in all three directions (see Fig. 1d). For each plane three different values of "pore width" were assumed, i.e. the effective distance between sheets (in y direction) – H_{eff} was equal to 0.8, 1.0, and 1.2 nm, respectively.

2.2 Geometric characteristics of considered systems

The porosity of the studied carbonaceous adsorbents was characterised by a geometrical method proposed by Bhattacharya and Gubbins (BG) [21]. The implementation of the method was described in detail elsewhere [19,22]. The accessible volume of pores (V_{acc}) was determined by the combination of Monte Carlo integration and the BG method

[19,22] i.e. only the volume of pores having the diameter above 0.3 nm was integrated. The arbitrarily assumed low limit (0.3 nm) is close to the size of CO_2 molecule.

For each slit-like system, the accessible surface area (S_{acc}) was also determined using VEGA ZZ 3.0.3.18 package [23-26]. We considered so-called van der Waals molecular surface (VdW). The probe radius was equal to 0.15 nm (the sphere analogical as applied during volume integration). During calculations the fast double cubic lattice method was used. For this method, the surface properties are calculated for each dot and its distance from the geometric center of the molecule (we assumed that the surface dot density is equal to 1000 for $Å^2$). VEGA ZZ can calculate and display some types of molecular surface through its 3D engine and it was successfully used in our previous studies [27,28].

2.3 Monte Carlo simulations of gaseous mixtures adsorption

For our studies, we chose two model binary gas mixtures: CO_2/CH_4 and CO_2/N_2. Adsorption at 298 K in the above-described boxes was modelled using the grand canonical Monte Carlo method (GCMC) [16,29]. Simulations were performed for the total mixture pressure equal to 0.1 MPa (i.e. atmospheric pressure) and for the following CO_2 mole fractions in gaseous phase y_{CO2} = 0.0, 0.01, 0.025, 0.05, 0.1, 0.2, 0.3, 0.4, 0.5, 0.6, 0.7, 0.8, 0.9, 0.95. 0.975, 0.99, and 1.0. Additionally, in order to check the separation of the mixtures for other pressures, we simulated adsorption of equimolar mixtures (y_{CO2} = 0.5) at different total pressure values in the range 1.0×10^{-6}-1.0 MPa. The methodology of calculations was analogous to that described previously [12]. Each GCMC simulation run consisted of 2.5×10^8 iterations. The first 1.0×10^8 iterations were discarded to guarantee equilibration. One iteration was an attempt of the system state change by the randomly selected perturbation: (i) displacement and/or rotation of randomly chosen molecule, (ii) creation of new molecule, (iii) annihilation of randomly chosen existing molecule or (iv) swap move with equal probabilities. We used equal probability for each perturbation to guarantee the condition of microscopic reversibility. Both the adsorbent structure and the molecules of adsorbate were modelled as rigid ones. Table 1 collects all applied values of the interaction parameters. Other computations details are given elsewhere [12,31,34].

From the GCMC simulation results, we determined the average numbers of each kind of adsorbate molecules in the simulation box ($\langle N_i \rangle$). These values were used for calculation of mole fractions of components in the adsorbed phase (x_i). Finally, in order to illustrate the

efficiency of mixture separation we also computed the values of equilibrium separation factors:

$$S_{1/2} = \frac{x_1/x_2}{y_1/y_2} \tag{3}$$

The adsorbed phase is enriched in the 1st component if $S_{1/2} > 1$. The isosteric enthalpy of adsorption (q^{st}) was also calculated (from the theory of fluctuations) to study the energetics of the process.

In addition, the adsorption of both mixtures (at total pressure equal to 0.1 MPa and different mole fractions) was simulated inside the series of 8 single-walled carbon zig-zag type nanotubes ((14,0) - (21,0)) for comparison. The characteristics of considered nanotubes are collected in Tab. S1 in Supplementary data. Each tube has the length of 6.345 nm. Periodic boundary conditions are applied along the tube axis formally mimicking the infinite nanotubes.

3. Results and discussion

Fig. S1b shows the changes in energy and animation 1 in Supplementary data presents the behaviour of carbon sheets during the equilibration process. As one can see we observe only a slight energy decrease. In the case of structures generated for small *A* values (*A* = 0.25 and 0.50 nm) geometry is almost unchanged in contrast to the structures generated for *A*= 0.75 and 1.00 nm which become more rounded.

From the data shown in Fig. 2 one can conclude that generally with the rise in the value of amplitude *A* adsorbed phase becomes more rich in CO_2. It is interesting, that there is a threshold *A* value (c.a. 0.5 nm) above which a remarkable rise in $S_{CO2/CH4}$ occurs. For a given *A* value the separation efficiency decreases with increasing pore width. Among studied pores, the highest efficiency of separation of CO_2 from the mixture with methane is observed for the pore having effective width equal to 0.8 nm. Generally for this smallest studied pore (H_{eff} = 0.8 nm) and for the largest *A* values (and *A* = 0.75 and 1.00 nm) the largest separation factors are recorded (see Fig. 2). This is accompanied by monotonically increasing enthalpy of adsorption values. One can see however, that around the y_{CO2} close to ca. 0.4, the curves for both pores intersect, and due to larger slope, the curve for *A* = 1.00 nm lies above this recorded for *A* = 0.75 nm. Cracknell et al. [35] while discussing the separation of CO_2/CH_4

mixture in the slit-like pores pointed out that to consider the changes in separation factors one should take into account the energetic and entropic factors, i.e. separation increases if the energy of adsorption increases and at the same time the lost of entropy should be small. As one can observe in Fig. 2 the enthalpy of adsorption for the considered pore is similar for the both considered A values but only for the y_{CO2} smaller than ca. 0.3. Above this value of y_{CO2} the enthalpy of adsorption in a pore with A = 1.00 nm still increases with y_{CO2}, however the enthalpy of adsorption in pore with A = 0.75 nm reaches a plateau. The details of the mechanism of this process are shown in animation 2 in Supplementary data comparing adsorption in both systems. From this movie it is seen that in the both studied systems two major configurations of CO_2 in pores are observed, i.e. monolayer in narrower part of pores (observed only in the system having A = 0.75 nm; note that in this case a monolayer is mainly created by CO_2 molecules) and polymolecular layer (created by the both molecules – CO_2 and CH_4) in the wider part of pores (observed in both systems i.e. for A = 0.75 and A = 1.00 nm). In the monolayer relatively large energy of adsorption is observed due to solid-fluid interactions, but at the same time there are strong restrictions in entropy of rotationally hindered CO_2 molecules [35]. Contrary in the polymolecular range molecules have larger entropy, they interact *via* fluid-fluid interactions, and this leads to progressive rise in the enthalpy of adsorption with the rise in y_{CO2}. Since this monolayer is (due to folding) not observed in pores having A = 1.00 nm the progressive rise in energy with pressure, due to strong fluid-fluid interactions occurs. Animation 2 (Supplementary data) clearly shows that above the intersection level of the both lines adsorption in pores having A = 0.75 nm is still mainly monomolecular, while in pores having A = 1.00 nm the filling of pores occurs.

The situation for pores with H_{eff} = 0.8 nm is similar for CO_2/N_2 mixture (Fig. 3, animation 3 in Supplementary data), but the intersection of selectivity curves for A = 0.75 nm and A = 1.00 nm occurs at smaller mole fractions of CO_2 in the gas phase (around y_{CO2} = 0.2). Also as in the case of CO_2/CH_4 mixture the enthalpy of adsorption monotonically increases with CO_2 mole fraction for A = 1.00 nm, and reaches a plateau above y_{CO2} = 0.2. Animation 3 in Supplementary data shows this situation and the explanation is analogous as for the case of CO_2/CH_4 mixture. It is worthy to note, that very high separation factors are recorded for this case, especially for A = 1.00 nm. This is mainly caused by smaller adsorption of nitrogen, comparing to methane.

The data presented in Figs. S2 and S3 in Supplementary data show a progressive rise in the separation factor with the rise in total mixture pressure, and as high values as around 50 for the mixture of CO_2 with nitrogen are recorded.

To discuss in detail the mechanisms of separation/adsorption the pore size histograms (calculated using the BG method) presented in Fig. 4 should be analysed. Since for a perfect slit-like pore only one pore diameter can be recorded, the BG method detects this diameter perfectly for all three analysed pores (see Fig. 4). However, with the rise in A value two effects are recorded, namely narrowing of the major pore and the appearance of smaller pores between graphene sheets (Fig. 4). Since the structural heterogeneity caused by folding is strictly related to the energetic heterogeneity this effect appears also in Fig. 5 presenting the potential energy of solid-fluid interactions maps. They are calculated for all three studied adsorbates in all studied pores. The data collected in Figs. 4 and 5 make it possible to explain relatively high $S_{i/j}$ factors observed in Figs. 2 and 3 (as well as Figs. S2 and S3 in Supplementary data), especially for high A values. One can see that for the smallest and the most folded studied nanopore (H_{eff} = 0.8 nm, A = 1.00 nm) all three molecules cannot access the narrowest part of the pore, due to repulsion (see also animations 2 and 3 in Supplementary data). Therefore they can be adsorbed only in the wider part of pores. Since the value of potential energy of CO_2 interaction with this part of pore is much higher than for CH_4 and N_2 separation factor is also high. As mentioned above, for small CO_2 mole fractions in the gas phase the highest separation factors are recorded for the pore with H_{eff} = 0.8 nm, and A = 0.75 nm (see Fig. 2). The potential energy profiles of solid-fluid interactions calculated for interaction of gases with studied pores explain observed situation (Fig. 5). As was mentioned above, in the monolayer region formed in the narrowest part of pore the highest energy of solid-fluid interactions is observed (see red places in Fig. 5). However the formation of a monolayer enables the appearance of strong fluid-fluid interactions, and this is why the enthalpy for adsorption in this system (see Fig. 2) is smaller than the enthalpy for the pore having A = 1.00 nm (here only polymolecular adsorption is observed - see above). By the way, high energy sites are also observed in the corners of pore having A = 1.0 nm (see Fig. 5). It is obvious that the decrease in pore width leads to decrease in the value of potential energy of solid-fluid interactions as it is shown in Fig. 5.

Finally a confirmation of the proposed regularities can be obtained from an analysis of selected snapshots collected on Fig. 6 and Figs. S4 and S5 in Supplementary data. The first two figures show the influence of A values (three arbitrarily chosen) on CO_2/CH_4 adsorption mechanism at constant total pressure (Fig.6) and for equimolar mixture at different p_{tot} (Fig. S4). One can easily observe how the adsorbed phase enriches with CO_2 with the rise in A and pressure values. The changes in mechanism of adsorption caused by the increase in pore

width (as an example equimolar CO_2/CH_4 mixture at p_{tot} = 0.10 and 1.00 MPa is shown) are presented in Fig. S5.

Finally, Fig. 7 compares the separation factors of both mixtures for, studied in this paper, folded pores and for single-walled carbon nanotubes. As was concluded in our previous study [1] there are two major factors important to reach high separation factor values, namely *S/V* ratio and the energy of solid-fluid interactions. The rise in the values of the both factors leads to the rise in $S_{i/j}$ value. Table 2 collects the geometric parameters for studied folded graphene structures. One can observe the progressive rise in *S/V* ratio with the rise in *A* value (the system H_{eff} = 0.8 nm and A = 1.00 is an exception - this is due to the fact that folding in this case leads to elimination of some parts of pore space at the places of pore walls contacts). With the rise in pore diameter the ratio *S/V* decreases. Also in this case the rise in tube diameters one can observe the progressive decrease in *S/V* ratio (Tab. S1 in Supplementary data). The efficiency of folded graphene slit like pores and nanotubes in separation of the both studied mixtures is shown in Fig. 7. One can see that for CO_2/CH_4 mixture folded graphene structures with comparable diameters to nanotubes show similar separation coefficients but have, at the same time, smaller *S/V* ratios. Thus for example tubes (15,0) and (16,0) having diameters 0.826 nm and 0.904 nm, respectively, have *S/V* equal to 4.842 and 4.426 1/nm. Folded graphene structures with width H_{eff} = 0.8 nm have *S/V* values equal to 3.649 and 3.237 1/nm for A = 0.75 nm and 1.00 nm, respectively. In the case of separation of CO_2/N_2 mixture similar separation factors are observed for folded graphene systems as for nanotubes having very close *S/V* ratios, however in this case nanotubes have larger diameters. The reason of this (neglecting the differences in energy of adsorption) is that in the case of folded graphene structures and CO_2/CH_4 mixture linear CO_2 molecules are effectively adsorbed in corners and heterogeneous places created by the folding of a pore, and this is no to so simple for spherical CH_4 molecules. Since such heterogeneous places are not present inside infinite nanotubes similar separation factors are observed for folded pores having smaller *S/V* ratios than nanotubes. However, in the case of CO_2/N_2 mixture both molecules are linear and have similar possibility to adsorb in corners, since the enhancement of separation as in the case of CO_2/CH_4 mixture does not occur.

4. Conclusions

In conclusion we show that folding of graphene pores (independent of pore width) is a promising method of increasing CO_2 separation from the mixtures with methane and nitrogen.

Our results suggest that the among studied systems, the best separation properties are observed for pores having an effective pore width 0.8 nm, and folding amplitude close to 1nm. We explain the mechanism of separation showing, that for the most effective pores mono and polymolecular layers are formed in nanopores. The comparison with nanotubes shows that folded graphene pores are very promising, especially for separation of CO_2/CH_4 mixture since the same separation factor values are reached for smaller *S/V* ratios. However, this situation does not occur for the second studied mixture (CO_2/N_2) where folding leads to similar separation factors as for nanotubes with comparable diameters and *S/V* ratios.

Acknowledgments

S.F., A.P.T. and P.A.G. acknowledge the use of the computer cluster at Poznań Supercomputing and Networking Centre (Poznań, Poland) as well as the Information and Communication Technology Centre of the Nicolaus Copernicus University (Toruń, Poland). S.F. gratefully acknowledges financial support from *Iuventus Plus* Grant No. IP2012 034872 from the Polish Ministry of Science and Higher Education.

References

[1] Furmaniak S, Terzyk A P, Kaneko K, Gauden P A, Kowalczyk P and Ohba T 2014 *Chem. Phys. Lett.* **595-596** 67

[2] Buseck P R, Huang B J and Keller L P 1987 *Energy Fuels* **1** 105

[3] Ugarte D 1992 *Chem. Phys. Lett.* **198** 596

[4] Gogotsi Y, Libera, J A, Kalashnikov N and Yoshimura M 2000 *Science* **290** 317

[5] Campos-Delgado J, Romo-Herrera J M, Jia X, Cullen D A, Muramatsu H, Kim Y A, Hayashi T, Ren Z, Smith D J, Okuno Y, Ohba T, Kanoh H, Kaneko K, Endo M, Terrones H, Dresselhaus M S and Terrones M 2008 *Nano Lett.* **8** 2773

[6] Liu Z, Suenaga K, Harris P J F and Iijima S 2009 *Phys. Rev. Lett.* **102** 015501

[7] Zhang J, Xiao J, Meng X, Monroe C, Huang Y and Zuo J-M 2010 *Phys. Rev. Lett*. **104** 166805

[8] Ju S-P, Chen K Y, Lin M C, Chen Y R, Lin Y L, Chang J-W and Huang S-C 2014 *Carbon* **77** 36

[9] Kim K, Lee Z, Malone B D, Chan K T, Alemán B, Regan W, Gannett W, Crommie M F, Cohen M L and Zettl A 2011 *Phys. Rev. B* **83** 245433

[10] Lopez-Bezanilla A, Campos-Delgado J, Sumpter B G, Baptista D L, Hayashi T, Kim Y A, Muramatsu H, Endo M, Achete C A, Terrones M and Meunier V 2012 *J. Phys. Chem. Lett.* **3** 2097

[11] Dutta D, Wood B C, Bhide S Y, Ayappa K G and Narasimhan S 2014 *J. Phys. Chem. C* **118** 7741

[12] Furmaniak S, Kowalczyk P, Terzyk A P, Gauden P A and Harris P J F 2013 *J. Colloid Interface Sci.* **397** 144

[13] Furmaniak S, Terzyk A P, Kowalczyk P, Kaneko K and Gauden P A 2013 *Phys. Chem. Chem. Phys.* **15** 16468

[14] Humphrey W, Dalke A and Schulten K 1996 *J. Mol. Graphics* **14** 33

[15] Harris P J F 1999 *Carbon Nanotubes and Related Structures* (Cambridge: Cambridge University Press)

[16] Frenkel D and Smit B 1996 *Understanding Molecular Simulation from Algorithms to Applications* (London: Academic Press)

[17] Marks N A 2000 *Phys. Rev. B* **63** 035401

[18] Marks N. 2002 *J. Phys.: Condens. Matt.* **14** 2901

[19] Furmaniak S 2013 *Comput. Methods Sci. Technol.* **19** 47

[20] Kowalczyk P, Furmaniak S, Gauden P A and Terzyk A P 2012 *J. Phys. Chem. C* **116** 1740

[21] Bhattacharya S and Gubbins K E 2006 Langmuir **22** 7726

[22] Furmaniak S, Terzyk A P, Gauden P A, Kowalczyk P, Harris P J F and Koter S 2013 *J. Phys.: Condens. Matt.* **25** 015004

[23] http://www.vegazz.net/

[24] Pedretti A, Villa L and Vistoli G 2002 *J. Mol. Graphics* **21** 47

[25] Pedretti A, Villa L and Vistoli G 2003 *Theor. Chem. Acc.* **109** 229

[26] Pedretti A, Villa L and Vistoli G 2004 *J. Comput.-Aided Mol. Des.* **18** 167

[27] Furmaniak S, Terzyk A P, Gauden P A, Wesołowski R P and Kowalczyk P 2009 *Phys. Chem. Chem. Phys.* **11** 4982

[28] Gauden P A, Terzyk A P, Furmaniak S, Harris P J F and Kowalczyk P 2010 *Appl. Surf. Sci.* **256** 5204

[29] Tylianakis E and Froudakis G E 2008 *J. Comput. Theor. Nanosci.* **6** 1

[30] Nguyen T X 2006 *Characterization of Nanoporous Carbons*, PhD thesis (Brisbane: University of Queensland)

[31] Terzyk A P, Furmaniak S, Gauden P A and Kowalczyk P 2009 *Adsorpt. Sci. Technol.* **27** 281

[32] Potoff J J Siepmann J I 2001 *AIChE J.* **47** 1676

[33] Steele W A 1974 *The Interaction of Gases with Solid Surfaces* (Oxford: Pergamon)

[34] Furmaniak S, Terzyk A P, Gauden P A, Harris P J F and Kowalczyk P 2009 *J. Phys.: Condens. Matt.* **21** 315005

[35] Cracknell R F, Nicholson D, Tennison S R and Bromhead J 1996 *Adsorption* **2** 193

Table 1.

The values of LJ potential parameters and point charges applied in simulations.

	Geometric parameters	**Centre**	**σ [nm]**	**ε/k_B [K]**	***q*/e**	**References**
CO_2	$l_{C=O}$ = 0.1162 nm	C	0.2824	28.680	+0.664	[30]
		O	0.3026	82.000	–0.332	
CH_4	$l_{C–H}$ = 0.1090 nm $\theta_{H–C–H}$ = 109°	C	0.3400	55.055	–0.660	[31]
		H	0.2650	7.901	+0.165	
		C-H[a]	0.3025	30.600	–	
N_2	$l_{N\equiv N}$ = 0.1100 nm	N	0.3310	36.000	–0.482	[32]
		COM[b]	–	–	+0.964	
graphene	$l_{C–C}$ = 0.1410 nm	C	0.3400	28.000	–	[33]

[a] cross-interaction parameters

[b] centre of mass

Table 2.

Geometric characteristics of all the considered simulation boxes constructed from the folded graphene sheets.

H_{eff}[a] [nm]	A [nm]	V_{acc} [cm^3/g]	S_{acc} [m^2/g]	S/V[b] [1/nm]
0.8	0.00	1.068	2678	2.509
	0.25	1.029	2660	2.586
	0.50	0.921	2664	2.893
	0.75	0.730	2664	3.649
	1.00	0.391	1266	3.237
1.0	0.00	1.326	2678	2.019
	0.25	1.282	2660	2.075
	0.50	1.155	2664	2.307
	0.75	0.930	2665	2.864
	1.00	0.523	1556	2.975
1.2	0.00	1.585	2678	1.689
	0.25	1.535	2660	1.733
	0.50	1.389	2664	1.918
	0.75	1.131	2665	2.356
	1.00	0.680	1885	2.773

[a] effective distance between parallel sheets (see Fig. 1d)

[b] surface to volume ratio

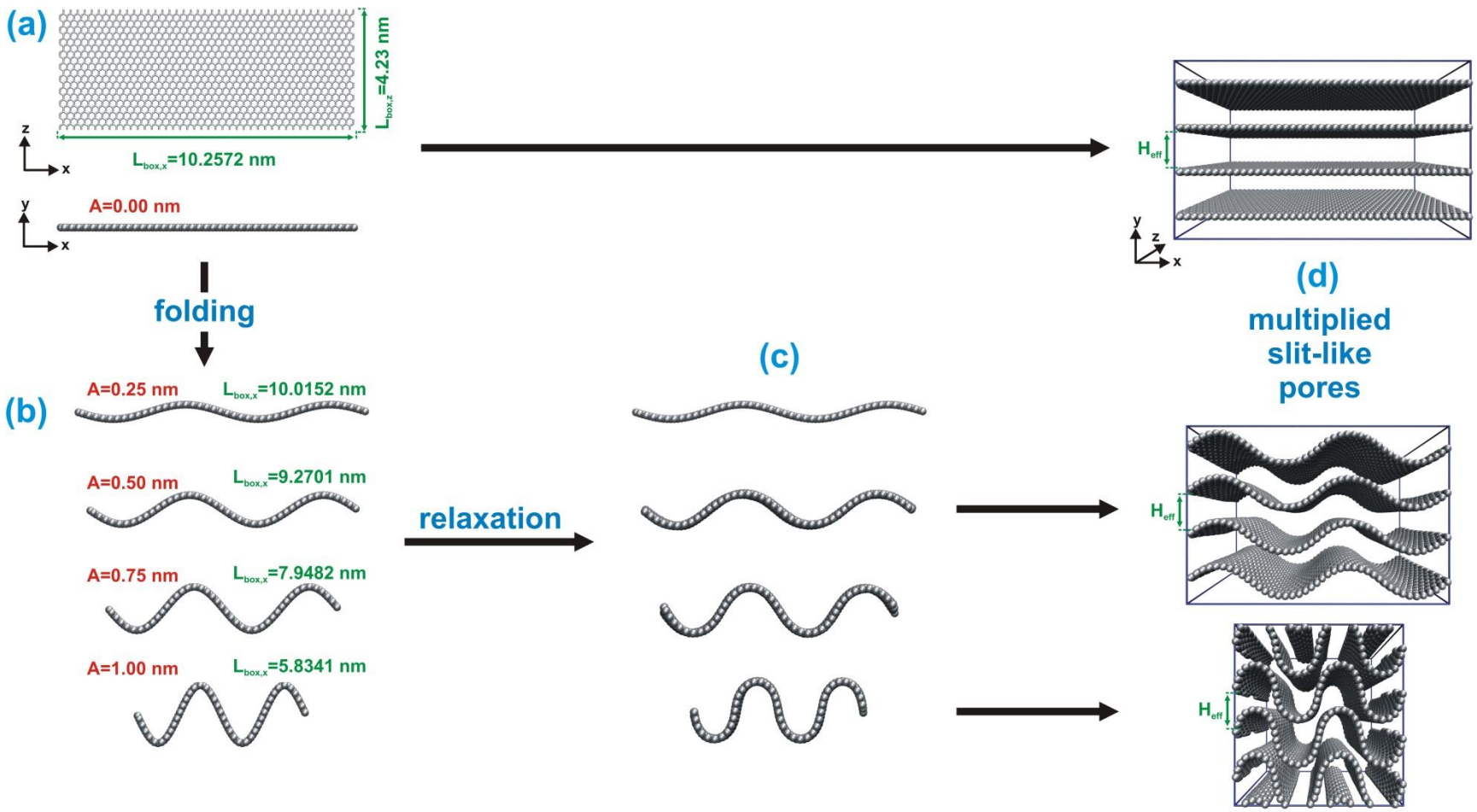

Figure 1. Schematic representation of the procedure applied to generate the simulation boxes with multiplied slit-like pores: (a) the starting graphene sheet, (b) folded sheets generated basing on Eq. (???) for all the considered values of amplitude (*A*), (c) the same planes after relaxation and (d) schematic representation of selected boxes (the frames reflect the size of the simulation box). It should be noted that this figure and all the snapshots and animations were created using the VMD program [14].

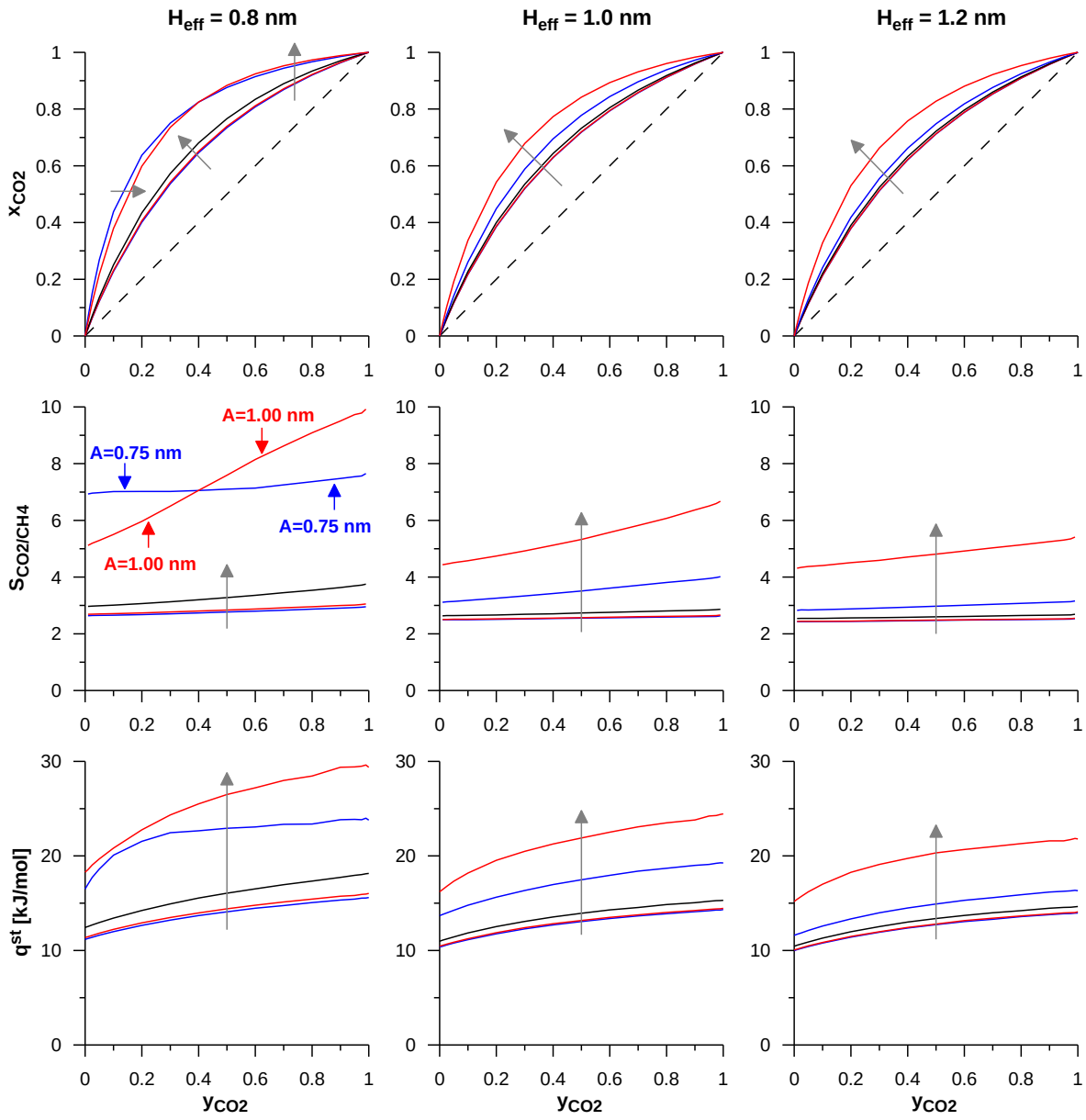

Figure 2. Comparison of the CO_2 mole fractions in adsorbed phase (x_{CO2}), the values of equilibrium separation factor ($S_{CO2/CH4}$) and isosteric enthalpy of adsorption (q^{st}) for all the considered systems plotted as the function of CO_2 mole fraction in gaseous phase (y_{CO2}) for adsorption of CO_2/CH_4 gas mixtures at the total pressure p_{tot} = 0.1 MPa. The gray arrows show the direction of changes related to the rise in the values of *A* parameter (i.e. the amplitude of sheets folding). The dashed lines on upper panels represent the CO_2 mole fraction in gaseous phase.

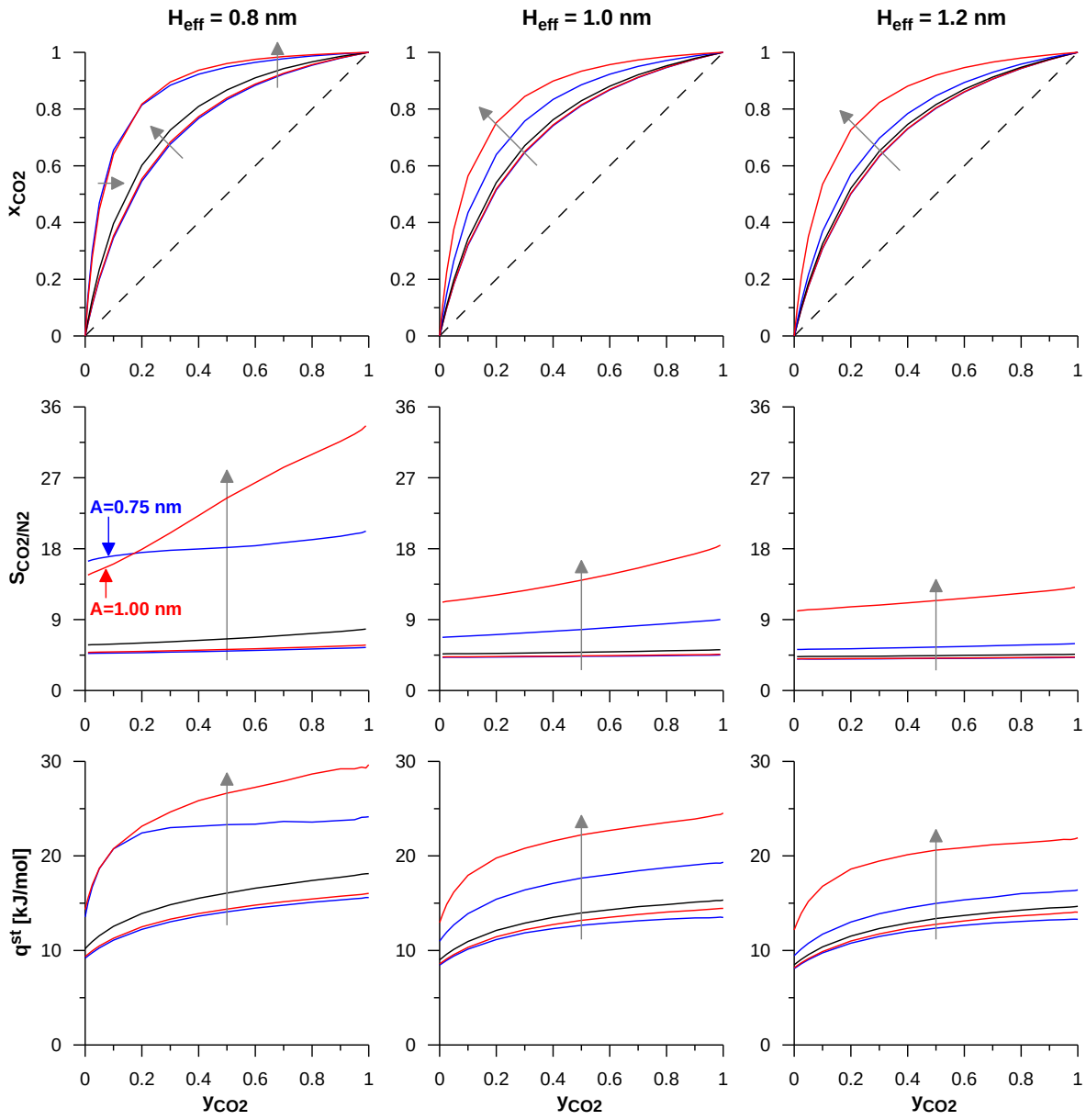

Figure 3. The same as in Fig. 2 but for adsorption of CO_2/N_2 mixtures.

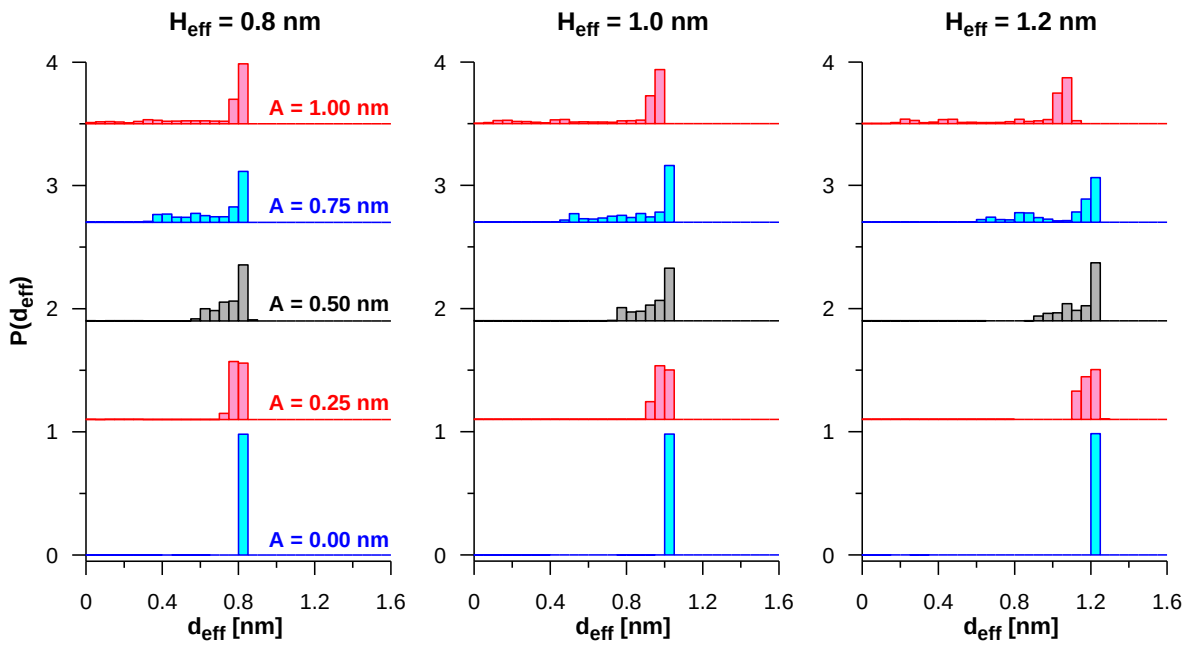

Figure 4. Comparison of the effective pore diameters (d_{eff}) histograms obtained from the application of the BG method for all considered systems. The subsequent histograms are shifted by 0.0, 1.1, 1.9, 2.7 and 3.5, respectively.

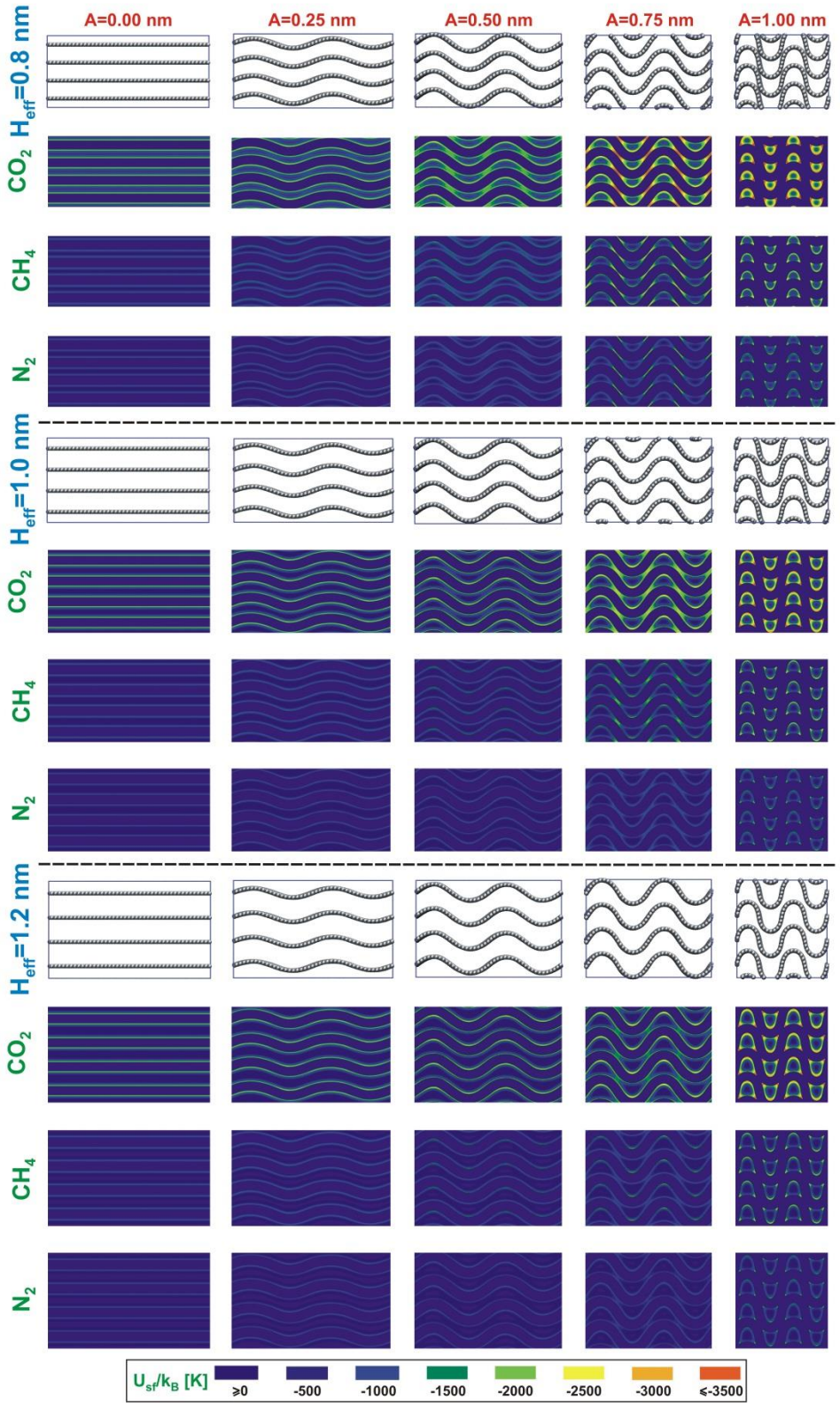

Figure 5. Comparison of solid-fluid interaction energy (U_{sf}) for three adsorbates in pores of all considered carbonaceous structures. For a molecule in a given location of its centre of mass, its angular orientation corresponding to the energy minimum was found in an iterative way.

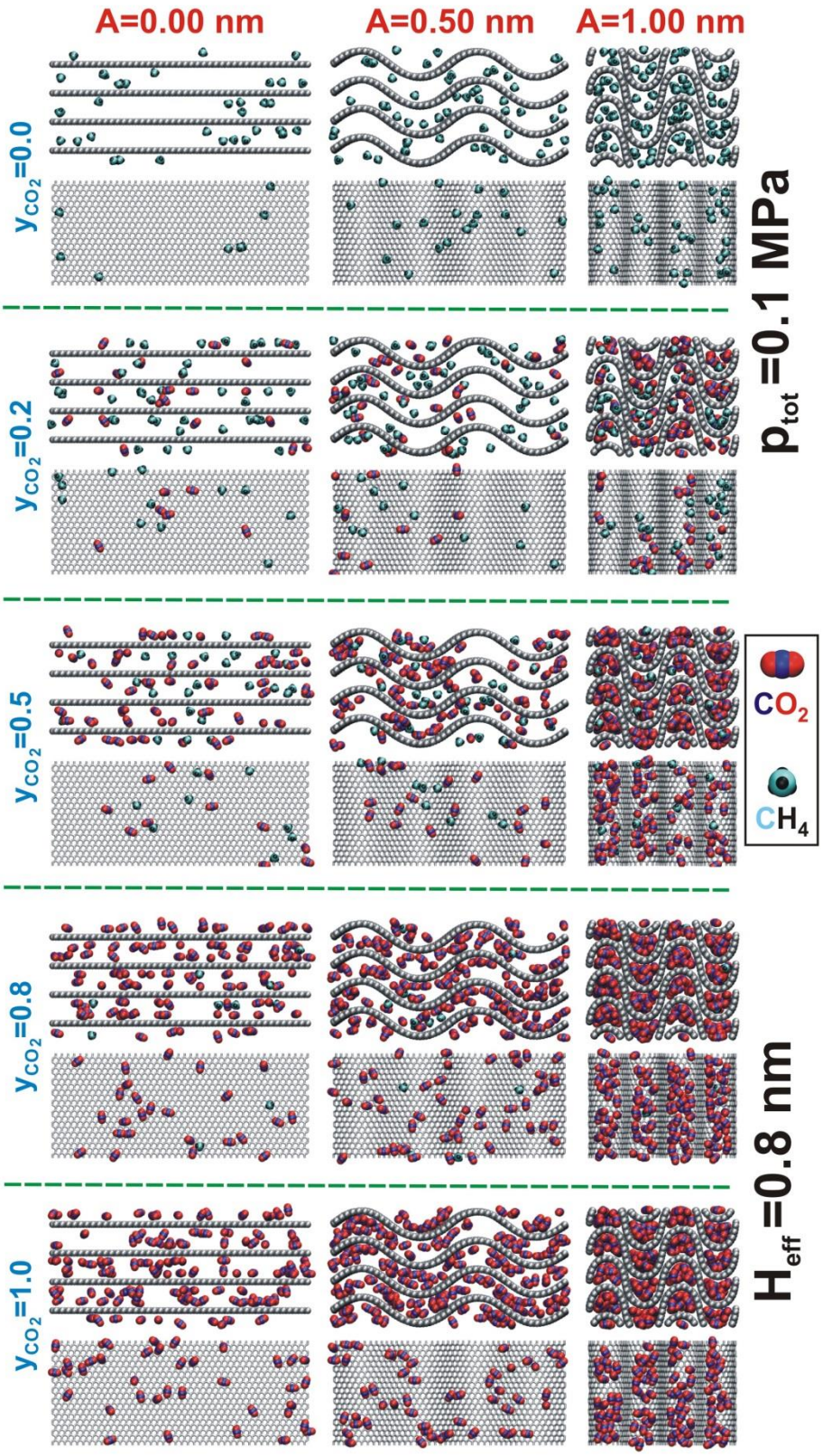

Figure 6. Selected equilibrium snapshots showing the configurations of molecules adsorbed inside the selected system (having the slit width H_{eff} = 0.8 nm) from the CO_2/CH_4 mixtures at the total pressure equal to 0.1 MPa for the selected mole fractions. The views on the whole box along the slits and from the top on the middle slit are shown.

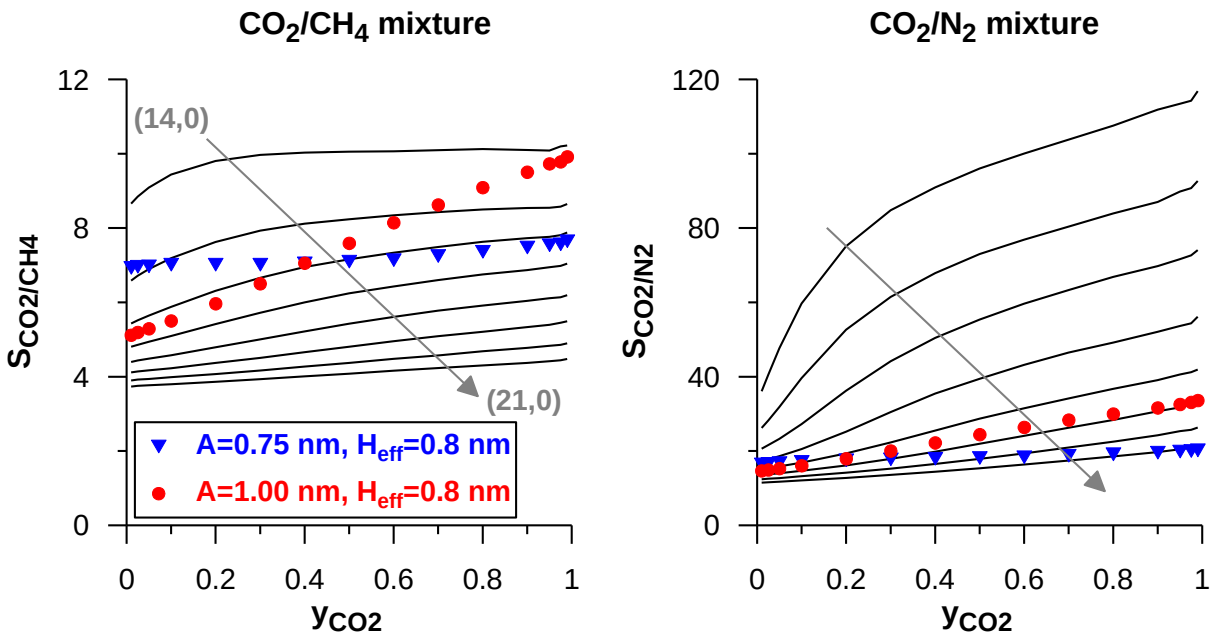

Figure 7. Comparison of equilibrium separation factors for adsorption of CO_2/CH_4 and CO_2/N_2 mixtures (at total pressure equal to 0.1 MPa) for two slit systems constructed from folded graphene sheets (both for H_{eff} = 0.8 nm and A equal to 0.75 or 1.00 nm, the data presented as points) and for single-walled carbon nanotube (the data presented as lines, the arrows show the direction of changes passing from the (14,0) nanotube up to (21,0) one).